Microporous and Mesoporous Materials 343 (2022) 112155

Contents lists available at ScienceDirect

Microporous and Mesoporous Materials

journal homepage: www.elsevier.com/locate/micromeso

Synthesis of organic–inorganic hybrids based on the conjugated polymer P3HT and mesoporous silicon

Natalia Gostkowska-Lekner [a,b,*], Danny Kojda [a], Jan-Ekkehard Hoffmann [a], Manfred May [c], Patrick Huber [c,d,e], Klaus Habicht [a,b], Tommy Hofmann [a]

[a] Helmholtz-Zentrum Berlin für Materialien und Energie GmbH, Hahn-Meitner Platz 1, D-14109 Berlin, Germany
[b] Institut für Physik und Astronomie, Universität Potsdam, Karl-Liebknecht-Str. 24-25, D-14476 Potsdam, Germany
[c] Hamburg University of Technology, Institute for Materials and X-ray Physics, Denickestr. 10, 21073 Hamburg, Germany
[d] Centre for Hybrid Nanostructures CHyN, University Hamburg, Luruper Chaussee 149, 22761 Hamburg, Germany
[e] Centre for X-ray and Nano Science CXNS, Deutsches Elektronen-Synchrotron DESY, Notkestr. 85, 22607 Hamburg, Germany

ARTICLE INFO

Keywords:
Mesoporous silicon
P3HT
Organic–inorganic hybrid
Melt infiltration

ABSTRACT

Organic–inorganic hybrids are a class of functional materials that combine favorable properties of their constituents to achieve an overall improved performance for a wide range of applications. This article presents the synthesis route for P3HT-porous silicon hybrids for thermoelectric applications. The conjugated polymer P3HT is incorporated into the porous silicon matrix by means of melt infiltration. Gravimetry, sorption isotherms and energy dispersive X-ray spectroscopy (EDX) mapping indicate that the organic molecules occupy more than 50% of the void space in the inorganic host. We demonstrate that subsequent diffusion-based doping of the confined polymer in a $FeCl_3$ solution increases the electrical conductivity of the hybrid by five orders of magnitude compared to the empty porous silicon host.

1. Introduction

Recent years saw the advent of conjugated polymers as promising functional materials for organic electronics. Organic semiconductors have received considerable attention in photovoltaics [1,2], photocatalysis [3,4], and optoelectronics [2,5]. They are also recognized as novel thermoelectric materials [6–9].

Organic semiconductors attract attention due to their tunable optical and electronic properties [10,11]. Advantages over inorganic materials are cost effectiveness and easy processability [12]. Additionally, their mechanical flexibility and lightweight allow for novel applications like wearable electronics [13] that cannot be realized with inorganic, heavy and rigid materials.

Several aspects challenge the large-scale implementation of polymer-based electronic devices up to date. Promising polymers often lack long-term stability, which is for instance a prerequisite for organic photovoltaics. Controlled doping and manufacturing reproducibility [14] are still challenging tasks. The lack of n-doped polymers [12] is of general concern. Overcoming these obstacles is a formidable task for conceiving market-ready technologies.

The combination of organic soft-matter and inorganic materials forms a bridge between conventional inorganic electronics and all-polymer based devices. The vision behind hybrids is to combine favorable properties of organic and inorganic constituents to enhance the performance beyond simple compound averages.

Many studies discuss organic–inorganic hybrids from an applied science point of view and cover a spectrum of topics [15–19], whose high diversity can only be reviewed exemplarily.

Studies by Gélvez-Rueda and Sofos illustrate the potential of hybrids for solar-energy harvesting [17,18]. Gélvez-Rueda [17] improved the charge-carrier separation in inorganic perovskite layers by incorporation of functional organic chromophores, whereas Sofos [18] synthesized alternating lamellar ZnO-conjugated molecule hybrids with improved photoconductive performance.

Improved thermoelectrics are promised by studies of Choi and Wang [19,20]. Choi designed a ternary hybrid of graphene/polymer/inorganic nanocrystal and observed double-carrier filtering at the two heterojunctions [20]. Wang found an exceptionally high power factor of $PF = 1350\,\mu W\,m^{-1}\,K^{-2}$ in (PEDOT)/Bi_2Te_3 hybrid films [19].

From a more fundamental point of view, functionalized molecules or polymers embedded in rigid, inorganic nanostructures are role models for nanoconfined soft matter. Their physical properties have

* Corresponding author at: Helmholtz-Zentrum Berlin für Materialien und Energie GmbH, Hahn-Meitner Platz 1, D-14109 Berlin, Germany.
E-mail address: natalia.gostkowska@helmholtz-berlin.de (N. Gostkowska-Lekner).

https://doi.org/10.1016/j.micromeso.2022.112155
Received 17 June 2022; Received in revised form 24 July 2022; Accepted 31 July 2022
Available online 13 August 2022
1387-1811/© 2022 The Author(s). Published by Elsevier Inc. This is an open access article under the CC BY license (http://creativecommons.org/licenses/by/4.0/).

to be carefully compared with the ones of their macroscopic bulk counterparts as spatial confinement affects the physical properties of soft matter [21,22] and consequently of the hybrids themselves. To provide a few examples, confinement is responsible for more effective electropolymerization of polyaniline inside silica pores than on bare ITO [23], modified chain orientations in pore-confined MEH-PPV polymers, which lead to novel optical properties [24], and nano-confinement induced chain alignment in poly (3-hexylotiophene) P3HT during thermal nanoimprinting [25], which is of obvious relevance for the inter-chain electronic conductance [14].

In this broad framework that motivates the synthesis of organic–inorganic hybrids, our study finds its roots in the field of thermoelectrics [19,20]. Thermoelectric materials will play a key role in a future energy infrastructure that is environmentally friendly and sustainable. They convert thermal energy into electrical energy and vice versa by means of Seebeck and Peltier effects. Large scale applications are waste heat recovery and refrigeration. Small scale applications are power supplies for wearable electronics in medical diagnostics or the entertainment sector [26,27]. All visionary applications however necessitate novel materials that excel in their performance over existing ones. In the ongoing effort to improve thermoelectric materials, organic–inorganic hybrids emerge as a possibility to overcome the drawbacks of conventional inorganic thermoelectrics that are the heavy weight, the temperature range of application, a lack of abundance, the high costs and often the need for toxic raw materials [28,29].

A distinct advantage of organic thermoelectrics is their flexibility and easy processability. They allow for near-room temperature application, a region that is merely covered by other materials. Mesoporous silicon exhibits intrinsically low thermal conductivity favorable for thermoelectrics due to increased phonon scattering at the pore boundaries. Its impaired electrical conductivity is a drawback but could be compensated by embedding conductive polymers with tunable electrical properties into the pore structure. Such hybrids could not only profit from beneficial properties of its constituents but ideally from synergy effects.

The motivations to use P3HT and pSi originate in their physical properties and more technical considerations like low complexity in synthesis. P3HT exhibits an exceptionally high charge carrier mobility [30], which can be enhanced by a factor of 20 upon chain alignment inside straight nanopores [31]. Solution and melt-based synthesis routes are favored by P3HT's solubility in chloroform, 2-chlorotoluene and toluene [32] and its low melting temperature of $T = 510\,\mathrm{K}$ [33].

Mesoporous silicon is a form of structured silicon characterized by nanometer-sized voids [34] in a crystalline Si matrix. It comes along with the promise to benefit from the technologically most advanced semiconductor industry of the arguably defining semiconductor material of the 20th and 21th century.

PSi is fabricated by electrochemical anodization in hydrofluoric acid (HF) based electrolytes. Pores in pSi are several tens of nanometers across and form networks with channels preferentially aligned along a particular crystallographic axis.

There are different strategies to fill the pores of pSi or, in general, nanostructured hosts with functionalized molecules. Wet-processing techniques such as dip-coating [35] are common approaches to incorporate polymers utilizing polymer solutions. Big challenges however are achieving homogeneous pore fillings as the removal of the solvent may cause redistribution of the active phase [36] and reaching a high degree of pore fillings for polymers with a large radius of gyration, respectively with low solubility.

Electropolymerization of monomers directly inside the pores [37–39] is a challenging bottom-up technique to fill pores with polymers of low solubility, large radius of gyration or polymers that dissociate before the melting point is reached.

Melt infiltration is conceptually the simplest approach. The viscous flow of the polymer melt into the pore channel is triggered by capillary forces. It depends mainly on the pore radius, surface tension, contact angle and viscosity. High degrees of pore filling can be achieved in a single step [36,40,41].

This article's description of the P3HT-pSi organic–inorganic hybrid (OIH) synthesis by means of melt infiltration is organized as follows. In the subsequent paragraphs, it describes the synthesis of pSi and the melt imbibition of polymers into the porous host. It continues with a discussion of the morphological properties of the synthesized OIH's before it highlights first measurements on electrical transport properties.

2. Experimental

2.1. Synthesis of mesoporous silicon

Mesoporous silicon is synthesized by means of electrochemical anodization in hydrofluoric acid (HF) based electrolytes. The source materials are single-crystalline boron-doped [100] Si wafers with a resistivity of $\rho = 0.01 - 0.02\,\Omega\,\mathrm{cm}$.

For electrochemical etching, we utilize a novel, custom-built anodization cell designed by Gostkowska-Lekner [42]. Electrolyte composition and anodization current are key synthesis parameters. Membranes for this study are anodized in HF/ethanol solution (HF(48 wt.%) : C_2H_6O (99.9 wt.%) = 4:6) with a constant current density of $j = 13\,\mathrm{mA\,cm^{-2}}$. An anodization time of 5 h leads to the growth of a 200 μm thick epilayer on the bulk Si wafer with pores roughly 9 nm across. The anodization ends with an increased current density of $j = 52\,\mathrm{mA\,cm^{-2}}$ for 40 s to detach the epilayer from the wafer and to obtain a self-supporting pSi-membrane.

2.2. Polymer infiltration into mesoporous Si

The regioregular (>90%) P3HT powder with low molecular weight $M_w = 2.0 \times 10^4 - 4.5 \times 10^4\,\mathrm{g\,mol^{-1}}$ was purchased from Sigma Aldrich™ and used as received. Adopting low molecular weight P3HT with a small radius of gyration reduces potential pore clogging [35].

The as-etched pSi membrane is heated up to 550 K, a temperature well above the melting point of P3HT ($T = 510\,\mathrm{K}$). The polymer powder placed on top of the heated membrane melts and flows into the nanochannels due to capillary forces [33]. The inset of Fig. 3 shows a sketch of the polymer imbibition in pSi.

The polymer flow in the nanochannels is an exceptionally slow process due to the high viscosity of the polymer liquid (99 Pa s) [43]. It takes up to 48 h to fill the pores of the membranes as discussed below in detail. After cooling to room temperature a residual P3HT layer is readily removed with a cotton pad and chloroform.

One should also note that the entire imbibition procedure is conducted in a glove box in an inert nitrogen atmosphere to avoid polymer oxidation and degradation upon exposure to illumination in air [44].

Conjugated polymers in their neutral stable state conduct electricity rather poorly. It is of importance to improve their electrical conductivity by means of doping to compete with the traditional inorganic semiconductors [45]. Solution-based chemical doping is one of the most popular and straightforward methods to incorporate counter ions into the polymer structure.

Synthesized hybrids are doped by immersion in saturated $FeCl_3$ chloroform solutions for 48 h or 72 h. The doping procedure takes place in a glove box under inert atmosphere.

P3HT doping prior to infiltration may cause unfavorable polymer aggregation. Solution doping after polymer infiltration bypasses any change in melt infiltration dynamics due to polymer morphological variation. The diffusion of Fe and Cl atoms into the confined polymer is further discussed in Section 3.4.

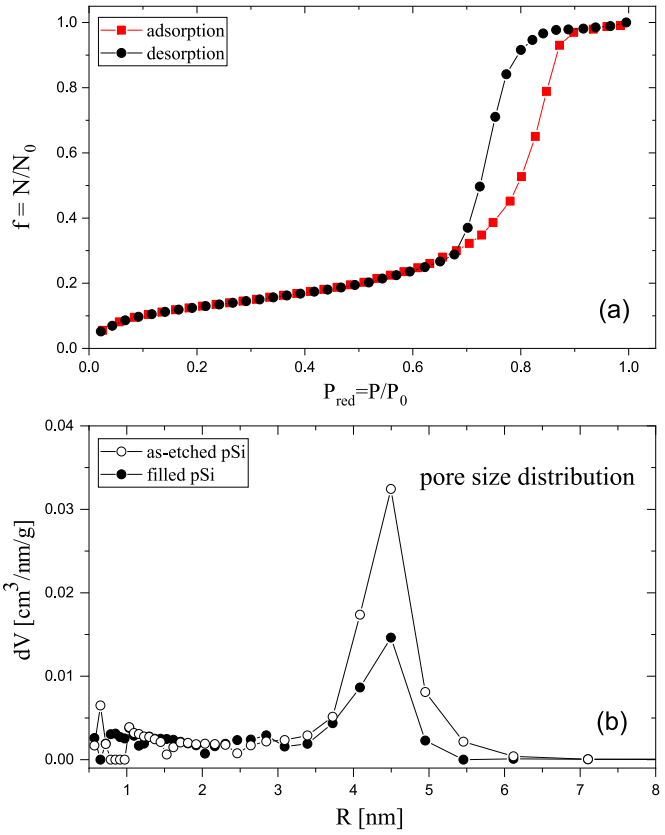

Fig. 1. (a) N_2 sorption isotherm of as-etched pSi at $T = 77$ K. (b) Pore-size distribution of as-etched membrane (open symbols) and vacant pore space after polymer imbibition (black symbols).

2.3. Characterization methods

2.3.1. pSi morphology

Nitrogen sorption isotherms are employed to characterize the morphology of mesoporous materials [46]. Isotherms probe the volumetric uptake of liquid nitrogen $f(P/P_0) = N/N_0$ inside the pore space at $T = 77$ K as the reduced pressure $P_{red} = P/P_0$ of the coexisting gas phase is step-wise changed. Here, N is the number of nitrogen molecules physisorbed and N_0 the number of molecules required to fill the pore volume completely. P and P_0 refer to equilibrium pressure of the confined liquid and saturation pressure of the bulk liquid.

The uptake as function of the reduced pressure P_{red} follows typically a hysteresis path upon adsorption and desorption (Fig. 1a). Multilayer formation on the pore walls at small reduced pressure is followed by capillary condensation at higher P_{red} with condensed liquid in the pore center. The physisorption data provide the pore-size distribution, effective surface area and porosity of the substrate by means of Brunauer–Emmet–Teller [47] and Barrett–Joyner–Halenda [48] analysis.

2.3.2. Polymer imbibition

Scanning electron microscopy (SEM) imaging is combined with energy dispersive X-ray spectroscopy (EDX) mapping utilizing a LEO GEMINI 1530 UltraPlus (Zeiss) electron microscope. It provides a direct visualization of the polymers in pSi (Fig. 3). Whereas SEM allows probing the morphology of the pSi cross-section itself, the EDX mapping identifies specific elements such as sulfur, carbon, iron or chloride in the probed region. Some of these elements are characteristic for the polymer only, e.g. sulfur. This element selectivity is exploited to reveal the polymer distribution in the membrane. It reveals (Fig. 3) in particular its depth profile from the membrane surface to the end of the propagating liquid polymer front.

One can define a degree of polymer filling f_p^{EDX} by means of the EDX signal depth profiles $I^{EDX}(x)$. Assuming that the EDX signal for selected elements is proportional to the amount of polymer in the pores and assuming that the pores on top of the membranes are filled completely, one obtains

$$f_p^{EDX} = \frac{\int I^{EDX}(x)dx}{I^{EDX}(0)\int dx}. \quad (1)$$

Gravimetry provides an alternative, quantitative estimate of the degree of polymer filling in the membranes. The weight of the empty membrane m_e, the weight of the filled membrane m_f and the pore volume V_p as obtained from the sorption isotherm predict a polymer filling f_p^{grav} of

$$f_p^{grav} = \frac{m_f - m_e}{\rho_{P3HT}} \frac{1}{V_p}. \quad (2)$$

The sorption isotherms of hybrids are also used to estimate the degree of filling. Estimating the empty pore volume V_p from sorption isotherms that are measured prior and post filling results in an polymer filling fraction f_p^{iso} of

$$f_p^{iso} = 1 - \frac{V_p^{post}}{V_p^{prior}}. \quad (3)$$

It is important to note that the polymer can block the access to smaller pores in the pore structure thus preventing the nitrogen to enter. The values of pore volume in this case would be underestimated, consequently the filling fraction overestimated.

2.3.3. Electrical transport

The electrical conductivity $\sigma(T)$ of the OIH samples is measured with an in-line four-probe technique using a commercial SBA 458 device (NETZSCH-Gerätebau GmbH) in the temperature range from 300 K to 373 K. Electrical contacts to inject a current of maximum 1 mA and to probe the voltage are placed on the cleaned sample side, that faced the polymer melt. $\sigma(T)$ is measured in helium atmosphere directly after transferring the samples from the glove box to the SBA device.

3. Results and discussion

This section discusses the morphology of as-etched as well as polymer-filled porous silicon membranes. The filling-factor determined with the methods presented in Section 2.3.2 is discussed. Filling-factor data of seven hybrids are presented to show the reproducibility of the synthesis.

3.1. As-etched membranes

The quantitative analysis of the N_2 sorption isotherms reveals a pore-size distribution in as-etched pSi membranes that centers around an average radius of $\overline{R} \approx 4.5$ nm with a standard deviation of not more than $\sigma(R) = 11\%$ (Fig. 1b). The porosity of the membranes is about 60% at a specific surface of $A = 382\,m^2\,g^{-1}$.

Fig. 2 shows a SEM micrograph of the pSi cross-section. The channels in mesoporous silicon are preferentially aligned along the [100] direction but exhibit numerous dendritic side branches that lead to an interconnected pore network [49]. Wider pores are interconnected via smaller channels.

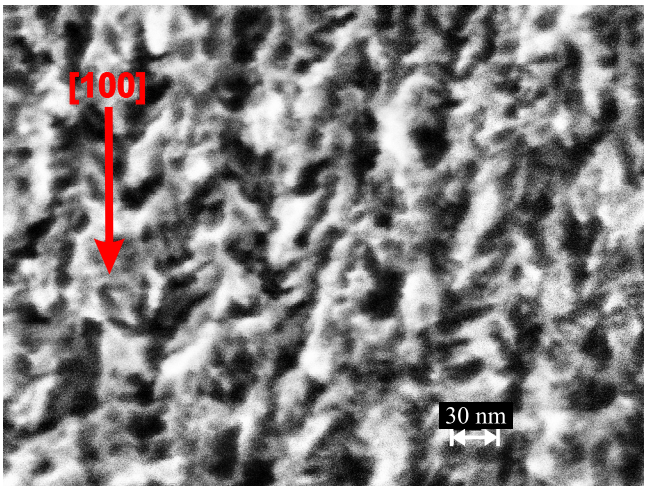

Fig. 2. SEM micrograph of the pSi cross-section along the [100] direction.

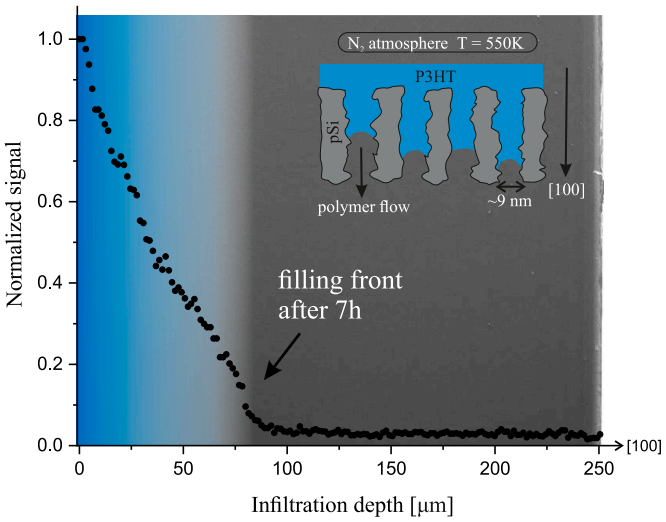

Fig. 3. PSi membrane partially filled with P3HT: Sample cross section and EDX sulfur signal (symbols) as function of depth. The membrane was etched for 6 h. The blue color indicates the filling region. The inset sketches the polymer flow into the pore space. (For interpretation of the references to color in this figure legend, the reader is referred to the web version of this article.)

3.2. Hybrids

Sorption isotherms, gravimetry and EDX spectroscopy stringently prove the successful physisorption of P3HT in the vacant pore space of pSi during the imbibition process. Fig. 1b is derived from the isotherms and already indicates that P3HT occupies roughly 50% of the pore space. A more quantitative analysis based on Eq. (3) confirms this qualitative assessment (see Table 1).

The degree of polymer filling obtained from the sorption isotherms is biased by pore clogging. The dendritic growth of the pores comes along with bottle necks between wider pores. These bottle necks and consequently some connected pores are not filled during imbibition. In particular, isolated islands of empty pore space within the otherwise filled substrate form. The volume of these islands is not probed by the N_2 isotherms due to a lack of access over the filled pore network. Therefore, f_p^{iso} is prone to overestimating the degree of pore filling.

Gravimetry provides no such uncertainty. The filling fractions f_p^{grav} for selected samples based on Eq. (2) is around $40\% < f_p^{grav} < 50\%$ as seen in Table 1. These values are marginally lower than the ones obtained from sorption isotherms.

EDX spectroscopy provides the most striking proof for successful P3HT imbibition. By the very design of the conceived synthesis route, the polymer melt flows into the pore network from the top of the membrane and a liquid polymer front propagates along the [100] crystallographic direction. As an instructive illustration, Fig. 3 shows the polymer filling at an intermediate state after 7 h.

The EDX sulfur signal, which is characteristic for the presence of P3HT, clearly evidences that the membrane is filled up to a depth of 80 μm and the sharp transition between filled and empty pSi is evident. In contrast, Fig. 4 indicates the presence of P3HT across the entire membrane after an imbibition time of 48 h.

The degree of filling based on the EDX signal appears less reliable than the one obtained by gravimetry and isotherms. To estimate the filling factor with EDX, the sulfur signal is integrated over the cross-section and normalized to the signal at the top of the membrane multiplied with the membrane thickness.

However, the underlying assumption, namely that the signal at the top of the membranes represents complete filling has to be taken with caution. It is experimentally almost inevitable to probe part of the membrane surface along the first few microns of the depth scan and consequently to overestimate $I^{EDX}(0)$.

As a result, filling fractions presented in Table 1 show roughly a factor of two decrease in filling compared to other methods. However, one might entertain the idea to properly calibrate the EDX signal with a gravimetric reference measurement.

It appears that the gravimetrically determined amount of pSi pore volume occupied by P3HT is the most accurate one. Together with nitrogen sorption isotherm measurements and SEM/EDX mapping there is no doubt about a successful infiltration of P3HT polymer into the mesoporous silicon membranes.

Some additional insights are gained from the fact that the strength of the sulfur signal decays continuously across the membrane. The most appealing explanation is that the imbibition involves two different time-scales [33,40]. In this scenario, the polymer melt wets the pore walls on a “fast” time scale as it creeps along the pore surfaces through the channels while the center remains empty. Then on a significantly “slower” time scale polymer in the pore center follows this precursor film.

In a less sophisticated explanation, one would assume that the polymer flow is increasingly impaired by bottle necks in the channels as the liquid front propagates along the pores. This could readily lead to a depth gradient in the polymer distribution and consequently a decaying EDX sulfur signal.

3.3. Reproducibility

An extended set of hybrids was synthesized under equal conditions. In particular, the infiltration time was always 48 h. These samples show no major difference in the filling factor (Table 1) and the polymer-specific EDX signals exhibit always the same decay characteristics as function of depth. As such, the discussed synthesis routes appear robust with highly reproducible outcome.

3.4. Doped hybrids

EDX mapping of the doped hybrids shows successful incorporation of $FeCl_3$ dopant atoms into the polymer matrix. In the element map of Fig. 4 one can distinguish the distribution of silicon, sulfur, iron and chlorine as a result of the discussed synthesis approach.

It is remarkable, that the signals from iron and chlorine which are characteristic of the dopant exhibit exactly the same decaying profile along the pore channels as the sulfur signal which is characteristic for the polymer. This clearly indicates successful diffusion of the doping agents into the polymer matrix contrary to physisorption of the $FeCl_3$ simply onto silicon pore walls or vacant pore space.

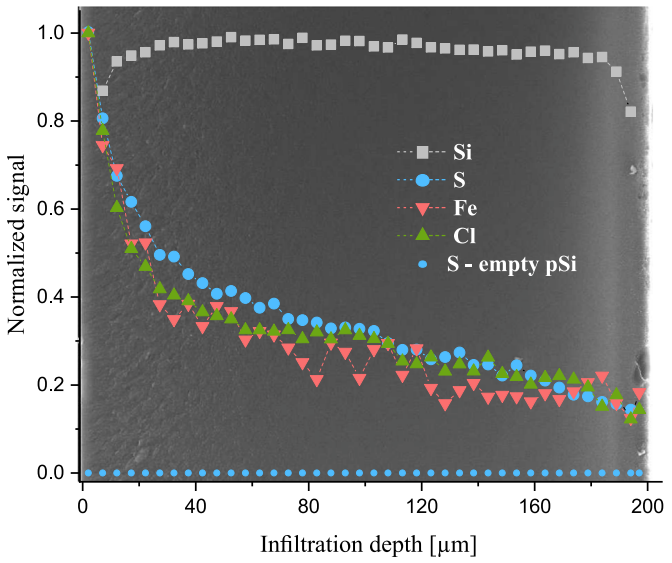

Fig. 4. Doped pSi-P3HT hybrid (48 h): EDX signals (symbols) of silicon, sulfur (P3HT), chlorine (dopant) and iron (dopant). The vanishing sulfur signal in the empty pSi membrane serves as reference. The background shows the membrane cross section.

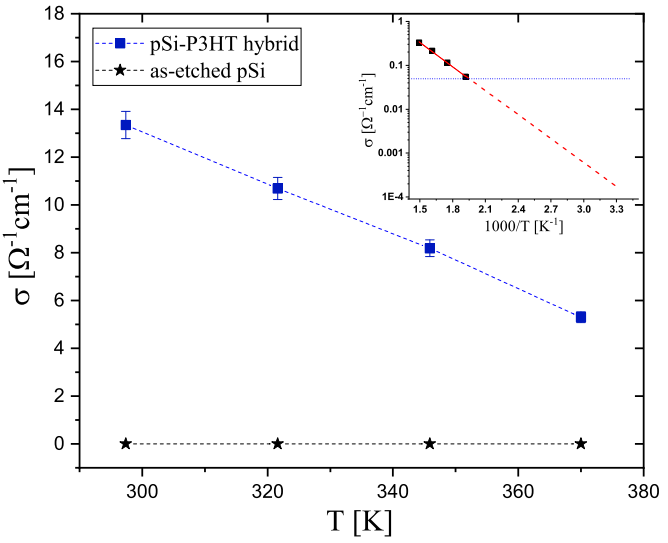

Fig. 5. Electrical conductivity of $FeCl_3$ doped hybrid and as-etched pSi. Inset: Arrhenius plot of as-etched membrane. The red dashed line is extrapolated from measurement data at high temperature (square symbols). The blue horizontal line marks the sensitivity limit of the device. (For interpretation of the references to color in this figure legend, the reader is referred to the web version of this article.)

3.5. Electronic transport

Electrical conductivity measurements on OIHs were performed in the temperature range between $T = 300\,\mathrm{K}$ and $T = 370\,\mathrm{K}$. In Fig. 5 a very low electrical conductivity is evident for the pSi matrix. Below 400 K the conductivity is even below the sensitivity limit of the used device that is $\sigma = 0.05\,\Omega^{-1}\,\mathrm{cm}^{-1}$ and shown data are a low temperature extrapolation. Assuming a thermally activated behavior the extrapolated data for room temperature conductivity is $\sigma(T = 300\,\mathrm{K}) = 10^{-4}\,\Omega^{-1}\,\mathrm{cm}^{-1}$

Preceding studies by Lee et al. [50] indicate for porous silicon with corresponding porosity a conductivity between $\sigma < 10^{-4}$–$10^{-3}\,\Omega^{-1}\,\mathrm{cm}^{-1}$ in the temperature range from $T = 300\,\mathrm{K}$ to $T = 370\,\mathrm{K}$. Compared with these studies and our low temperature extrapolation, the conductivity of the selected hybrids is remarkably increased by five orders of magnitude compared to pSi in the same T–range. It is $\sigma(T = 300\,\mathrm{K}) = 13\,\Omega^{-1}\,\mathrm{cm}^{-1}$.

Additionally to this phenomenal increase in conductivity, it is also intriguing to note the different temperature dependence of the electrical conductivity. As the inset in Fig. 5 shows, the electrical conductivity in pSi is thermally activated. It increases exponentially with temperature. On the contrary, the electrical conductivity of OIHs decreases with temperature. This contrast resembles the situation encountered in undoped and doped semiconductors.

It is up to subsequent studies to interpret the temperature dependent conductivity of pSi and OIH's in detail. The exponentially increased conductivity in pSi might be explained in terms of T-dependent free charge-carrier densities and phonon-assisted carrier hopping. Complementary measurements of OIHs Hall-mobility will show whether the decreasing conductivity in hybrids relates to increased carrier scattering at elevated temperatures. Seebeck coefficient measurements will provide more comprehensive insights into charge transport and the improved performance of the OIH.

4. Conclusions and outlook

The presented study is a very first step in an ambiguous attempt to synthesize organic–inorganic thermoelectric hybrids and to fundamentally understand their thermoelectric transport properties on a macroscopic and microscopic level.

Table 1
Filling factor for 48 h infiltration time: comparative characterization based on sorption isotherms, gravimetry, and EDX cross-section scan.

Small area samples (>50 mm²):	Sorption isotherm	Gravimetry	EDX
Hybrid 1	49,8%	41%	19%
Hybrid 2	55%	45%	21%
Large area samples (<50 mm²): Synthesized for SBA measurements			
Hybrid 3	–	55%	30%
Hybrid 4	–	52%	31%
Hybrid 5	–	50%	28%
Hybrid 6	–	45%	22%
Hybrid 7	–	37%	19%

We have demonstrated in this mindset successful synthesis of hybrids based on P3HT conductive polymer and free standing 200 μm thick porous silicon. Organic molecules are introduced into 9 nm wide pores by means of melt infiltration. Sorption isotherm, gravimetry and EDX mapping convincingly show that the P3HT occupies roughly 50% of the pore space. Upon polymer doping with $FeCl_3$, the electrical conductivity of the resulting hybrid is significantly enhanced compared to mesoporous silicon.

As the project goes on, one must focus on the link between microscopic structure and thermoelectric functionality of the successfully synthesized hybrids. These investigations are a prerequisite for any meaningfully devised application. The measurement of electrical and thermal conductivity, Hall mobility and Seebeck effect will provide a full thermoelectric characterization of the hybrids. X-ray and neutron scattering techniques come to mind providing information on an ultrastructural level. They are suited to identify the morphology of the polymer in the confining host – a significant parameter that defines its functionality – and they should be able to probe the structure of the polymer/silicon interfaces as important for charge and heat transport through the hybrid. Scattering studies might be complemented by TEM characterization and solid-state NMR. In a nutshell, one can conclude that tempting experiments are ahead.

The results from our fundamental studies on the hybrids provide a sound basis to help understanding the basic functionality of this new material class. In particular, they will help to evaluate the potential of organic–inorganic hybrids for thermoelectrics. Whether the envisioned

application as energy converter or small-scale electronics will find industrial approval requires further studies, demonstrating upscaling of the synthesis routes for large scale production, as well as a thorough evaluation of device performance.

CRediT authorship contribution statement

Natalia Gostkowska-Lekner: Writing – review & editing, Writing – original draft, Methodology, Investigation, Formal analysis, Conceptualization. **Danny Kojda:** Writing – review & editing, Methodology. **Jan-Ekkehard Hoffmann:** Writing – review & editing, Methodology. **Manfred May:** Writing – review & editing, Methodology. **Patrick Huber:** Writing – review & editing, Project administration. **Klaus Habicht:** Writing – review & editing, Writing – original draft, Supervision, Resources. **Tommy Hofmann:** Writing – review & editing, Writing – original draft, Supervision, Resources, Project administration, Formal analysis, Conceptualization.

Declaration of competing interest

The authors declare that they have no known competing financial interests or personal relationships that could have appeared to influence the work reported in this paper.

Data availability

Data will be made available on request.

Acknowledgments

We thank the DFG, Germany for funding the project Hybrid thermoelectrics based on porous silicon: Linking Macroscopic Transport Phenomena to Microscopic Structure and Elementary Excitations, project number 402553194.

References

[1] H. Bin, L. Gao, Z.-G. Zhang, Y. Yang, Y. Zhang, C. Zhang, S. Chen, L. Xue, C. Yang, M. Xiao, Y. Li, Nature Commun. 7 (2016) 1–11.
[2] U.-Y. Cheng, S.-H. Yang, C.-S. Hsu, Chem. Rev. 109 (2009) 5868–5923.
[3] B. Muktha, G. Madras, T.N. Guru Row, U. Scherf, S. Patil, J. Phys. Chem. B 111 (2007) 7994–7998.
[4] M. Zhanga, X. Wang, Energy Environ. Sci. 7 (2014) 1902–1906.
[5] C.R. McNeill, N.C. Greenham, Adv. Mater. 21 (2009) 3840–3850.
[6] M. Bharti, A. Singh, S. Samanta, D.K. Aswal, Prog. Mater. Sci. 93 (2018) 270–310.
[7] B. Russ, A. Glaudell, J. Urban, M.L. Chabinyc, R.A. Segalman, Nat. Rev. Mater. 1 (2016) 1–14.
[8] H. Yao, Z. Fan, H. Cheng, X. Guan, C. Wang, K. Sun, J. Ouyang, Macromol. Rapid Commun. 37 (2018) 1–22.
[9] G. Kim, L. Shao, K. Zhang, K.P. Pipe, Nature Mater. 12 (2013) 719–723.
[10] I. Piquero-Zulaica, A. Garcia-Lekue, L. Colazzo, C.K. Krug, M.S.G. Mohammed, Z.M. Abd El-Fattah, J.M. Gottfried, D.G. De Oteyza, J.E. Ortega, J. Lobo-Checa, ACS Nano 12 (2018) 10537–10544.
[11] H. Masai, J. Terao, Polym. J. 49 (2017) 805–814.
[12] J.A. Rivera, A.C. Castillo, M.D.L.L.M. Gonzalez, Organic semiconductors, in: Semiconductors, Springer Nature, Switzerland, 2019.
[13] P.C.Y. Chow, T. Someya, Adv. Mater. 32 (2020) 1–26.
[14] H. Peng, X. Sun, W. Weng, X. Fang, Polymer Materials for Energy and Electronic Applications, Elsevier, 2017.
[15] Y. Du, S.Z. Shen, K. Cai, P.S. Casey, Prog. Polym. Sci. 37 (2012) 820–841.
[16] S.H. Mir, L.A. Nagahara, T. Thundat, P. Mokarian-Tabari, H. Furukawa, A. Khosla, J. Electrochem. Soc. 165 (2018) B3137–B3156.
[17] M.C. Gélvez-Rueda, M.B. Fridriksson, R.K. Dubey, W.F. Jager, W. van der Stam, F. Grozema, Nature Commun. 11 (2020) 1–9.
[18] M. Sofos, J. Goldberger, D.A. Stone, J.E. Allen, Q. Ma, D.J. Herman, L.J. Tsa2, W.-W. Lauhon, S.I. Samuel I. Stupp, Nature Mater. 8 (2009) 68–75.
[19] L. Wang, Z. Zhang, Y. Liu, B. Wang, L. Fang, J. Qiu, K. Zhang, S. Wang, Nature Commun. 9 (2018) 1–8.
[20] J. Choi, J. Lee, S.-S. Lee, C. Park, H. Kim, Adv. Energy Mater. 6 (2016) 1–8.
[21] P. Huber, J. Phys.: Condens. Matter 27 (2015).
[22] O. Gang, P. Huber, A. Karim, I. Zvonkina, S.-W. Lee, J.-W. Kim, D.K. Roper, W.J. Li, Soft Matter and Biomaterials on the Nanoscale, Vol. 1, World Scientific, 2020.
[23] F. Montilla, M.A. Cotarelo, E. Morallon, J. Mater. Chem. 19 (2009) 305–310.
[24] I.B. Martini, I.M. Craig, W.C. Molenkamp, H. Miyata, S.H. Tolbert, B.J. Schwartz, Nature Nanotechnol. 2 (2007) 647–652.
[25] M. Aryal, K. Trivedi, W. Hu, ACS Nano 3 (2009) 3085–3090.
[26] A. Dahiya, F. Morini, S. Boubenia, K. Nadaud, D. Alquier, G. Poulin-Vittrant, Adv. Mater. Technol. 3 (2018) 1700249.
[27] C. Xin, Z. Hu, Z. Fang, M. Chaudhary, H. Xiang, X. Xu, L. Aigouy, Z. Chen, Mater. Today Energy 22 (2021) 100859.
[28] H. Jin, J. Li, J. Iocozzia, X. Zeng, P.-C. Wei, C. Yang, N. Li, Z. Liu, J. Hau He, T. Zhu, J. Wang, Z. Lin, S. Wang, Angew. Chem. 58 (2019) 15206–15226.
[29] M. Kemerink, C. Müller, M.L. Chabinyc, M. Brinkmann, Appl. Phys. Lett. 119 (2021) 260401.
[30] H. Sirringhaus, P. Brown, R. Friend, M.M. Nielsen, K. Bechgaard, B.M.W. Langeveld-Voss, A.J.H. Spiering, R.A.J. Janssen, E.W. Meijer, P. Herwig, D.M. de Leeuw, Nature 401 (1999) 686–688.
[31] K.M. Coakley, B.S. Srinivasan, J.M. Ziebarth, C. Goh, Y. Liu, M.D. McGehee, Adv. Funct. Mater. 15 (2005) 1927–1932.
[32] M. Roesing, J. Howell, D. Boucher, J. Polym. Sci. B: Polym. Phys. 55 (2017) 1075–1087.
[33] J. Martín, A. Nogales, M. Martín-González, Macromolecules 46 (2013) 1477–1483.
[34] V. Lehmann, R. Stengl, A. Luigart, Mater. Sci. Eng. B 69 (2000) 11–22.
[35] S.L. Lim, Y. Liu, G. Liu, S.Y. Xu, H.Y. Pan, E.-T. Kang, C.K. Ong, Phys. Status Solidi (A) 208 (2011) 658–663.
[36] P.E. De Jongh, T.M. Eggenhuisen, Adv. Mater. 25 (2013) 6672–6690.
[37] D. Kowalski, P. Schmuki, Chem. Commun. 46 (2010) 8585–8587.
[38] N.C. Strandwitz, Y. Nonoguchi, S.W. Boettcher, G.D. Stucky, Langmuir 26 (2010) 5319–5322.
[39] M. Brinker, G. Dittrich, C. Richert, P. Lakner, T. Krekeler, T.F. Keller, N. Huber, P. Huber, Sci. Adv. 6 (2020) 1–8.
[40] L.G. Cencha, G. Dittrich, P. Huber, C.L.A. Berli, R. Urteaga, Phys. Rev. Lett. 125 (2020) 234502.
[41] F. Vazquez Luna, M. Gerstenberger, G. Dittrich, J. Martins de Souza e Silva, P. Huber, R. Wehrspohn, M. Steinhart, J. Phys. Chem. C 125 (2021) 26731–26743.
[42] N. Gostkowska-Lekner, D. Wallacher, N. Grimm, K. Habicht, T. Hofmann, Rev. Sci. Instrum. 91 (2020) 1–6.
[43] J. Fanous, M. Schweizer, D. Schawaller, M. Buchmeiser, Macromol. Mater. Eng. 297 (2012) 123–127.
[44] S. Cook, A. Furubea, R. Katoh, J. Mater. Chem. 22 (2012) 4282–4289.
[45] P. Kar, Doping in Conjugated Polymers, Wiley, 2013.
[46] M. Thommes, K. Kaneko, A. Neimark, J. Olivier, F. Rodriguez-Reinoso, J. Rouquerol, K. Sing, Pure Appl. Chem. 87 (2015) 1051–1069.
[47] S. Brunauer, P.H. Emmett, E. Teller, J. Am. Chem. Soc. 60 (1938) 309–319.
[48] E.P. Barrett, L.G. Joyner, P.P. Halenda, J. Am. Chem. Soc. 73 (1951) 373–380.
[49] R. Smith, S. Collins, J. Appl. Phys. 71 (1992) R1–R22.
[50] W.H. Lee, C. Lee, J. Jang, J. Non-Cryst. Solids 198–200 (1996) 911–914.